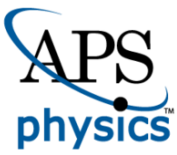

Regulating Brownian Fluctuations with Tunable Microscopic Magnetic Traps

A. Chen, G. Vieira, T. Henighan, M. Howdyshell, J. A. North, A. J. Hauser, F. Y. Yang, M. G. Poirier, C. Jayaprakash, and R. Sooryakumar

Phys. Rev. Lett. **107**, 087206 — Published 18 August 2011

DOI: 10.1103/PhysRevLett.107.087206

Regulating Brownian Fluctuations with Tunable Microscopic Magnetic Traps

A. Chen, G. Vieira, T. Henighan, M. Howdyshell, J. A. North, A. J. Hauser, F. Y. Yang, M. G. Poirier, C. Jayaprakash, and R. Sooryakumar

Department of Physics
The Ohio State University
Columbus, OH 43210.

A major challenge to achieving positional control of fluid borne submicron sized objects is regulating their Brownian fluctuations. We present a magnetic-field-based trap that regulates the thermal fluctuations of superparamagnetic beads in suspension. Local domain-wall fields originating from patterned magnetic wires, whose strength and profile are tuned by weak external fields, enable the bead trajectories within the trap to be managed and easily varied between strong confinements and delocalized spatial excursions that are described remarkably well by simulations.

Nature has proven that it is possible to engineer complex nano-scale machines in the presence of thermal fluctuations [1-4]. These biological complexes, which harness random thermal energy to provide functionality, yield a framework to develop artificial, i.e. non-biological, phenomena and devices. Indeed, thermally activated transitions in optical traps [5], diffusion in solids through activated escape from metastable states [6-8] and transport of colloidal particles [9] and DNA [10] through a combination of diffusive and electric forces are examples where the ceaseless source of thermal motion is channeled into useful outcomes. An important outcome of controlling thermally driven motion in a fluid (i.e. Brownian fluctuations) will be the ability to manipulate and generate deterministic motion of individual objects in the 100 nm to 10 micron range. Indeed, several approaches to achieve this goal have been implemented – such as optical tweezers [11], dielectric tweezers [12], and electrokinetic traps [13] – each with its own advantages and drawbacks.

Although the trapping of paramagnetic objects in a stable, solely magnetic configuration in free space is not possible [14], control of their Brownian fluctuations in quasi three- or two-dimensions exclusively through magnetic fields would nevertheless provide much added value. The wide tunable force range, convenience of remote access and selectiveness to objects with designed magnetic signatures is of high interest. In this letter we demonstrate a non-contact way of regulating Brownian fluctuations of magnetic beads of micron to sub-micron size that is based on a recently developed platform used to transport labeled biological cells [15]. Critical to this regulation is the underlying principle of combining a weak external magnetic field **(**$|\mathbf{H}_{\mathbf{ext}}|$~100 Oe) and fields generated from domain walls ($\mathbf{H}_{\mathbf{dw}}$) residing in ferromagnetic wires designed on a silicon

surface (Fig. 1(a)). We show that such a superposition of fields enables the bead to execute stochastic motion within a tunable deterministic quasi-3D trapping potential such that that the position of its energy minimum can be manipulated along a predetermined pathway, and its depth varied from several to a few k_BT (thermal energy). This remote control on the local energy landscape enables Brownian fluctuations to be varied from being tightly confined (virtually immobilizing the bead) to undergoing large excursions (expediently biased away from the wire vertex where a domain wall resides).

Figure 1(b) illustrates the wire-patterned Si platform supporting a solution of magnetic beads that consist of small (~10 nm) iron oxide nanoparticles embedded in a polymer matrix with radius R = 0.28 μm or 0.6 μm. A key property of the beads is their superparamagnetic character [16] that enables them to be readily magnetized in fields of only a few tens of Oersted at room temperature and display no remnant magnetization. The magnetic moment, **M**(H), of the bead is induced by the net field $\mathbf{H} = \mathbf{H_{dw}} + \mathbf{H_{ext}}$, where three-dimensional control of the external field $\mathbf{H_{ext}} = (H_x, H_y, H_z)$ is achieved by the electromagnets and coil as shown in Fig. 1(c). The interaction between **M** and **H** leads to a deterministic trapping force on the bead while thermal fluctuation leads to its stochastic motion. We follow the motion of the bead in trapping potentials subjected to different external fields through an optical microscope with a 40x objective lens. A CCD camera and tracking routines resolve individual trajectories with sub-micron resolution.

Figure 2 provides an overview of the central results. In the absence of $\mathbf{H_{ext}}$ (row (i)), strong field gradients (>10^4 T/m) from the domain wall confine a bead (R = 0.28μm) to the vertex. The computed vertical force F_z (~ -27 pN ≈ -6,500 k_BT/μm), pushes the bead towards the surface. The calculated potential depth was $\Delta U \approx 527\ k_BT$ with spring

constants $k_x = k_y \approx 96$ pN/μm ≈ 23,000 $k_BT/\mu m^2$. We find the resulting fluctuation in bead position is below our measurement resolution of ~100 nm, consistent with the calculated root-mean-square (rms) displacement of 9.3nm due to thermal fluctuations.

Application of an in-plane field on the order of tens of Oersted (e.g. $H_x = 0$ and $H_y = 35$ Oe) breaks the symmetry, shifting the trap away from the vertex in the same direction as the in-plane field (+y), while a field in the -z direction (e.g. $H_z = -74$ Oe) weakens the trap. The resulting net field leads to a local field maximum and potential energy minimum that is formed at $y \approx 0.3$ μm from the vertex center (row (ii)). Concomitantly, the trap was also weakened (ΔU to 22 k_BT; $F_z = -1{,}200$ $k_BT/\mu m$, $k_x = 1{,}400$ $k_BT/\mu m^2$, and $k_y = 250$ $k_BT/\mu m^2$ at the minimum) and became anisotropic. Both the simulation and experiment (last two columns) showed a tightly confined bead trajectory near the vertex tip at this field value. As shown in row (ii)-(iv), when H_z was progressively decreased (-74 → -86 → -91 Oe), the energy minimum moved farther away ($y \approx 0.3 \rightarrow 0.7 \rightarrow 0.8$ μm) from the wire vertex, while the depth ΔU further weakened (ΔU ≈ 22 → 10 → 8 k_BT; $F_z \approx -1{,}200 \rightarrow -140 \rightarrow -110$ $k_BT/\mu m$, $k_x \approx 1{,}400 \rightarrow 72 \rightarrow 45$ $k_BT/\mu m^2$, and $k_y \approx 250 \rightarrow 74 \rightarrow 53$ $k_BT/\mu m^2$ at the respective minima.)

As evident in both simulation and experiment (last two columns of Fig. 2), the weakening of the asymmetric trap causes an increase in the extent of Brownian motion of the bead. The bead remained in the focal plane of the objective lens as long as the sum of the vertical force provided by the trap and the buoyant weight (~0.1 $k_BT/\mu m$ for R = 0.28 μm; ~1.5 $k_BT/\mu m$ for R = 0.6 μm) was strong enough to confine the bead near to the surface. In row (iv), the vertical trapping force dropped below 1 $k_BT/\mu m$ for $y > 4$ μm so

that the bead could become momentarily out of focus when it was far away from the energy minimum (Movie 3 in Supplemental Materials [17]).

Row (v) in Fig. 2 demonstrates the ability of this platform to confine Brownian motion of a bead of radius R = 0.6 μm functionalized with a short DNA (20 base pairs) tethered to it. DNA attachment was confirmed by fluorescence of DNA-conjugated dye molecules. As expected since the DNA is short, we observed no qualitative difference between the DNA tethered and non-tethered beads of the same radii in their Brownian motion and response to the tunable trap. The more confined motion of the R = 0.6 μm bead compared to the 0.28 μm bead in traps of similar depth ($\Delta U \approx 8k_BT$) can be attributed to the fact that the diffusion coefficient scales as 1/R.

Figure 3 shows the detailed dependence of the extent of the Brownian motion (for R = 0.28 μm) on the strength of the anisotropic trap by plotting the average (dots) and rms fluctuations (vertical bars) in the y-position of the bead trajectory as a function of the tuning field H_z, while keeping H_x=0 and H_y=35 Oe fixed. As H_z is decreased from -70 to -90 Oe, the distribution of Brownian trajectory shifts gradually along +y direction, while extending its spread in the range of $0 \le y \le 2$ μm. Upon further decreasing H_z below -90 Oe, experiment and theory revealed an abrupt increase in fluctuation up to 10~15 μm, due largely from the more frequent escapes of the bead to the flatter region of the energy landscape (i.e. row (iv) of Fig. 2).

We describe the motion of the bead by Langevin dynamics [18,19] where viscous damping due to the fluid dominates the inertial forces. The center-of-mass (**r**) of the bead satisfies the Langevin equation

$$6\pi\eta R\frac{d}{dt}\mathbf{r} = -\nabla U + \mathbf{f}(t) \ ,$$

where the left-hand side is the frictional Stokes force on the bead due to the fluid, and **f**(t) is a Gaussian white noise with variance $12\pi\eta R k_B T$, representing thermal fluctuations. The deterministic force arises from the interaction energy U(r) between the moment of the bead and the net field **H**(**r**):

$$U(\mathbf{r}) = -\mu_0 V \int_{H(\infty)}^{H(\mathbf{r})} M(H')dH',$$

where M(H) and V are the field induced magnetization and volume of the bead respectively. The energy landscapes in Fig. 2 were based on calculation of U in the plane of z = R wherein a useful quantitative measure of the asymmetric trap and its influence on the bead trajectories at temperature T is provided by $\Delta U/k_B T$. Here $\Delta U = U(\infty) - U_{min}$ is the difference in the potential energy minimum and the potential at a distant location. Since M(H) changes monotonically with H, the energy minimum coincides with the field maximum. Although M(H) only serves to modulate U(**r**), due to a log-normal size distribution of the embedded nanoparticles in the bead [20], the resulting M(H) (modeled as a superposition of classical moments) is non-linear in H, i.e. susceptibility χ not constant, even at low H (<100 Oe), as seen in the inset of Fig. 3(a). This reduction in χ causes further weakening of the trap as the tuning field changes. The contribution of the domain wall field $\mathbf{H_{dw}}$ to the net field **H** was, for computational simplicity, approximated as that generated from a magnetic monopole [21] located at the center of the vertex. This serves as an excellent description for $\mathbf{H_{dw}}$, except in the immediate vicinity of the vertex, where the precise domain wall structure would influence the local field.

The overall scale of the bead magnetization M(H) is difficult to determine due to the uncertainty in the exact nanoparticle size distributions within the bead and the precise

wire magnetization. For the experimentally determined values of various parameters and the appropriate model of the monopole strength, the semi-quantitatively reproducible behaviors of the bead are strikingly similar to the experimental results as shown in the fourth and fifth columns of Fig. 2 as well as Fig. 3.

The increase in the extent of Brownian motion as H_z is decreased (toward more negative) (Fig. 3) can be understood from Boltzmann statistics, i.e. the ensemble-averaged probability for the bead to be located at **r** is proportional to $\exp[-(U(\mathbf{r})-U_{min})/k_BT]$. As ΔU decreases the particle can be found farther from the energy minimum and the extent of the trajectory increases. When ΔU becomes comparable to k_BT, the bead has a higher probability to overcome the deterministic potential barrier on the time scale of interest (i.e. 5 minutes); large excursions of Brownian trajectories with motion biased away from the zigzag wires then happen more frequently (row (iv) Fig. 2). In the experiments, we track single trajectories for a particular realization of the noise term **f**(t) and so ensemble averages were not performed in the simulations.

A significant advantage of a solely magnetic trap as presented here is the ability to remotely tune its relative strength with weak external magnetic fields without altering the fluid environment, such as local heating or the need to adjust the dielectric property of the fluid as in optical or dielectric tweezers. Although a potential drawback of this approach is the requirement for a magnetic signature on the entity being manipulated, magnetic nanoparticles could be embedded directly within or attached to inert or biological (e.g. DNA) entities of interest. While other approaches based on magnetic fields have utilized Brownian fluctuations to characterize trapping forces [22, 23] and susceptibility of the beads [24], the method presented here serves as an experimental implementation of a

magnetic trap that provides a high degree of control over the extent of the Brownian fluctuation of the bead and a quantitative understanding of the parameters that influence it. This allows us to selectively suppress the low-frequency components (in free Brownian motion, the power spectrum of the noise is white and the mean-square deviation of the position increases linearly in time) thereby controlling local areal coverage of the trajectories. In addition to low cost and biocompatibility, this approach allows multiple beads to be loaded at different vertices in fluid environment for concurrent trapping, control, and easy observation with a standard optical microscope.

In conclusion, a fundamental challenge in the advancement of nanotechnology is the development of precision tools for the manipulation and transport of nano-objects and biomolecules in solution. The tunable magnetic trap presented here with the feature of controlling the relative importance between the deterministic and stochastic (Brownian) forces helps achieve this goal. Underlying this control are: 1) embedded superparamagnetic nanoparticles that display a non-linear response to magnetic fields, 2) monopole-like high gradient (10^4 T/m) fields produced by magnetic wires imprinted on a platform, and its delicate combination with 3) weak external fields of only tens to a hundred Oersted that tune the trap. These ingredients enable the bead dynamics to be easily varied between tightly confined and delocalized spatial excursions. As demonstrated by the quantitative understanding of the stochastic dynamics and the ability to manipulate a DNA-tethered bead, our experiments open many possibilities for basic and applied research in both nanoscience and molecular biology.

This material is based upon work supported by the U.S. Army Research Office under contract W911NF-10-1-0353.

Figure Captions

FIG. 1. Experimental setup: (a) Schematic of $Co_{0.5}Fe_{0.5}$ zigzag wires of rectangular cross-section on a silicon surface. Typical wire width and thickness were 2μm and 13.5 nm respectively. The magnetization ($\mathbf{M_{wire}}$) points towards or away from the vertices, generating monopole-like fields ($\mathbf{H_{dw}}$) that attract magnetic beads to the vertices. (b) Platform: The O-ring and cover-slip prevent fluid flow and evaporation of solution of paramagnetic beads. (c) Schematic of electromagnets and coil to generate fields H_x, H_y, and H_z in the x, y, and z directions respectively. Platform was observed by a microscope (40x objective lens). A CCD camera recorded the trajectories of the bead.

FIG. 2. Trapping individual superparamagnetic beads in solution. *Left column:* Bead of radius R = 0.28 μm (row (i)-(iv)) and DNA-tethered bead with R = 0.6 μm (row (v)). *Second column:* Orientation of the external field $\mathbf{H_{ext}} = (0, H_y, H_z)$ with respect to zigzag wire. Head-to-head configuration of magnetizations on neighboring arms of wire ($\mathbf{M_{wire}}$) generates out-going domain wall field $\mathbf{H_{dw}}$. *Third column:* Calculated energy landscapes and their potential depth ΔU for beads in the presence of $\mathbf{H_{dw}}$ and corresponding $\mathbf{H_{ext}}$. The wire vertex and energy contours (in 1.9 k_BT increments) are projected on top of the energy landscape. *Fourth and fifth columns:* Simulated and experimentally observed bead trajectories under corresponding field conditions. Each simulation and experiment was for a period of 5 minutes, except for the experiment in row (iv), which was for 3 minutes. See Supplemental Materials [17] for movies for each experiment, including an additional movie recorded under fluorescence mode for the DNA-tethered bead (Movie 5).

FIG. 3. Average position (dots) and rms fluctuation (vertical bars) of the R = 0.28 μm bead trajectory in the y-direction as a function of H_z, keeping $H_x = 0$ and $H_y = 35$ Oe fixed. Each data point is obtained from a single 5-minute trajectory, except for field value (iv) which was a 3-minute trajectory. Arrows labeled with (ii)-(iv) correspond to external field values in Fig. 2. (a) Results of the simulation: Inset shows calculated magnetization M(H) (modeled as a superposition of classical moments [20]) of the superparamagnetic bead as a function of net field H, with dots indicating values at the energy minimum formed under external field values (ii)-(iv). Note non-linearity of the M(H) curve at low H (~100 Oe). (b) Results of the experiment.

References

[1] P. Hänggi and F. Marchesoni, Rev. Mod. Phys. **81**, 387–442 (2009).

[2] R. D. Astumian, Science **276**, 917-922 (1997).

[3] G. Oster, Nature **417**, 25-25 (2002).

[4] R. F. Fox, Phys. Rev. E **57**, 2177–2203 (1998).

[5] L. I. McCann, M. Dykman, and B. Golding, Nature **402**, 785-787 (1999).

[6] P. Hänggi, P. Talkner, and M. Borkovec, Rev. Mod. Phys. **62**, 251–341 (1990).

[7] M. I. Dykman and D. Ryvkine, Phys. Rev. Lett. **94**, 070602 (2005).

[8] D. G. Luchinsky *et al.*, J. Phys. A: Math. Gen. **32**, L321-L327 (1999).

[9] J. Rousselet *et al.*, Nature **370**, 446-448 (1994).

[10] J. S. Bader *et al.*, Proc. Nat. Acad. Sci. **96**, 13165-13169 (1999).

[11] A. Ashkin *et al.*, Opt. Lett. **11**, 288-290 (1986).

[12] B. Edwards, N. Engheta, and S. Evoy, J. Appl. Phys. **102**, 024913-5 (2007).

[13] A. E. Cohen and W. E. Moerner, Proc. Nat. Acad. Sci. **103**, 4362-4365 (2006); Appl. Phys. Lett. **86**, 093109 (2005); A. E. Cohen, Phys. Rev. Lett. **94**, 118102 (2005).

[14] S. Earnshaw, Trans. Camb. Phil. Soc. **7**, 97 (1842).

[15] G. Vieira *et al.*, Phys. Rev. Lett. **103**, 128101-4 (2009).

[16] I. S. Jacobs and C. P. Bean, in *Magnetism*, edited by G. T. Rado and H. Suhl (Academic, New York, 1963), Vol. 3, p271.

[17] Supplemental Materials: *Movies 1-4* correspond to field conditions in the experiments shown in row (ii)-(v) of Fig 2. *Movie 5*, recorded in fluorescence mode, corresponds to experiment shown in row (v) of Fig. 2 but with a slightly

different external field of $\mathbf{H}_{ext}$ = (0,21 Oe,-111 Oe). All movies have been sped up 10 times. In each movie, $\mathbf{H}_{ext}$ was set to 0 for the first 5 seconds (real time) and then set to (0,Hy,0) for the next 5 seconds before being adjusted to the final value, e.g. (0,35 Oe,-74 Oe) in Movie 1.

[18] P. Langevin, C. R. Acad. Sci. (Paris) **146**, 530-533 (1908).

[19] W. Horsthemke and R. Lefever, *Noise Induced Transitions: Theory and Applications in Physics, Chemistry and Biology* (Springer-Verlag, Berlin, 1984).

[20] G. Mihajlović *et al.*, Appl. Phys. Lett. **91**, 172518 (2007).

[21] J. D. Jackson, *Classical Electrodynamics, 3rd ed.* (Wiley, New York, 1998), pp. 278-279.

[22] E. Mirowksi *et al.*, Appl. Phys. Lett. **84**, 1786 (2004).

[23] L. E. Helseth *et al.*, Langmuir **20**, 6556 (2004).

[24] K. van Ommering *et al.*, Appl. Phys. Lett. **89**, 142511 (2006).

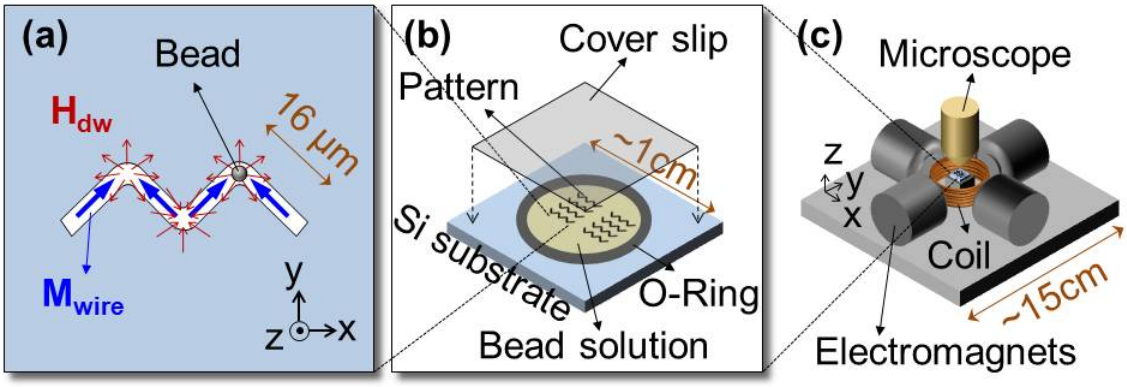
(a)
Bead
H_{dw}
16 μm
M_{wire}
y
z
x
(b)
Cover slip
Pattern
~1cm
Si substrate
O-Ring
Bead solution
(c)
Microscope
z
y
x
Coil
~15cm
Electromagnets

Figure 1

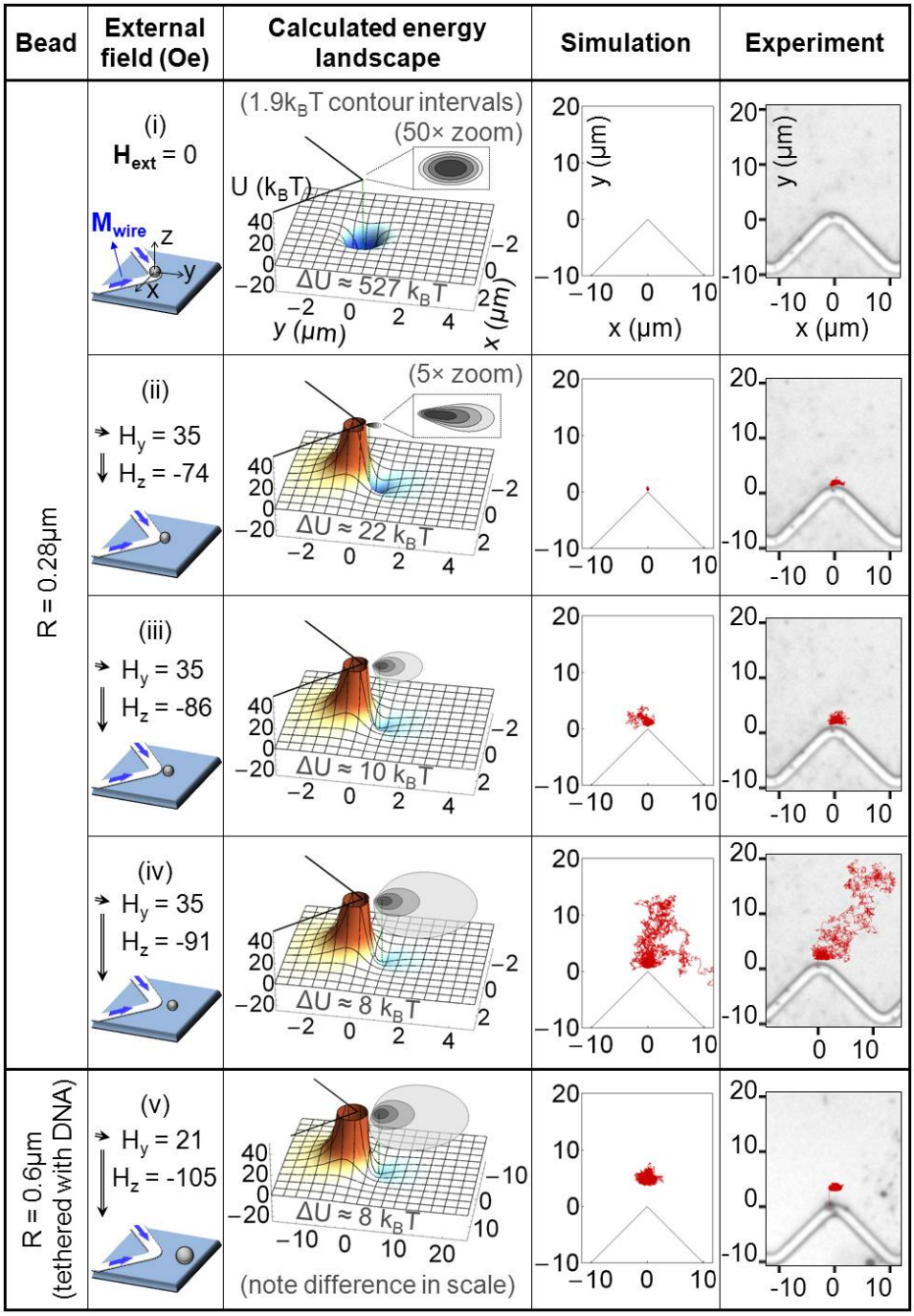
Bead
External field (Oe)
Calculated energy landscape
Simulation
Experiment
R = 0.28μm
R = 0.6μm (tethered with DNA)
(i)
H_ext = 0
M_wire
z
y
x
(1.9k_BT contour intervals)
(50× zoom)
U (k_BT)
ΔU ≈ 527 k_BT
y (μm)
x (μm)
(ii)
H_y = 35
H_z = -74
(5× zoom)
ΔU ≈ 22 k_BT
(iii)
H_y = 35
H_z = -86
ΔU ≈ 10 k_BT
(iv)
H_y = 35
H_z = -91
ΔU ≈ 8 k_BT
(v)
H_y = 21
H_z = -105
ΔU ≈ 8 k_BT
(note difference in scale)

Figure 2

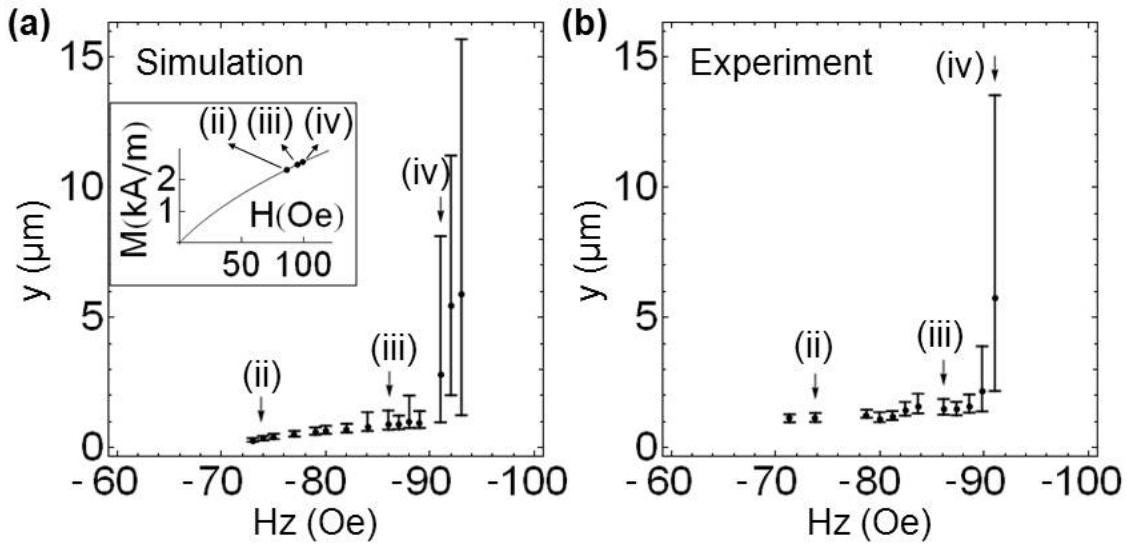
(a)
Simulation
(ii) (iii) (iv)
M(kA/m)
2
1
H(Oe)
50 100
(iv)
(iii)
(ii)
y (μm)
15
10
5
0
-60 -70 -80 -90 -100
Hz (Oe)
(b)
Experiment
(iv)
(ii)
(iii)
y (μm)
15
10
5
0
-60 -70 -80 -90 -100
Hz (Oe)

Figure 3